# Pulsed aerosol-assisted plasma processes for (multi)functional thin film deposition

G Carnide, L Cacot, M Feron, V Pozsgay, M L Kahn, C. Villeneuve-Faure, H Caquineau, N Naudé, L Stafford, R Clergereaux

# Pulsed aerosol-assisted plasma processes for (multi)functional thin film deposition

G. Carnide[1,2], L. Cacot[1,3], M. Feron[1], V. Pozsgay[1],
M.L. Kahn[2], C. Villeneuve[1], H. Caquineau[1], N. Naudé[1], L. Stafford[3] and R. Clergereaux[1]

[1] *Laboratoire Plasma et Conversion d'Energie - Laplace, CNRS-Université de Toulouse, France*
[2] *Laboratoire de Chimie de Coordination - LCC, CNRS, Toulouse, France*
[3] *Département de Physique, Université de Montréal, Canada*

**Abstract:** Pulsed aerosol injection is an appealing method to inject complex precursors in plasmas independently on their composition and thermodynamic characteristics. This method is implementable to form (multi)functional thin films in various plasma processes by pulse injecting colloidal solutions or by using a pulsed direct liquid reactor-injector of nanoparticles. However, the pulsed injection introduces new specific physics.

**Keywords:** Aerosols, Pulsed Direct Liquid Injection, Plasma Deposition, Safer-by-design.

## 1. General

Plasma Enhanced Chemical Vapor Deposition (PE-CVD) enable to form various thin films. Initially focused on gases, the injection of liquid precursors vapors for few decades enabled to breaks down few technological barriers of PE-CVD. For example, the injection of organosilicon precursors resolved the problems of powdering and security purposes related to silane-based processes [1]. Nowadays, various organometallic molecules, *i.e.* molecular species containing metal atoms (including silicon) bonded with organic compounds are used as precursors for thin film deposition of organosilicon [2], silica [3], organotitanium [4] or zirconia [5], etc. However, such precursors need to be first volatile. Indeed, to ensure an efficient injection and deposition process, the molecules should have a vapor pressure of several Pa at room temperature or at temperatures below its decomposition temperature [6] In addition, it needs to be stable during storage, manipulation, and use, which limits the range of materials that can be prepared.

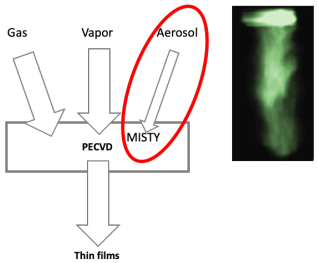


Fig. 1. Strategies for (multi)functional thin film plasma deposition. An image of aerosol taken by rapid imaging is reported inset.

An alternative deals with aerosol-assisted processes (Fig. 1). Indeed, aerosols are suspensions of micrometric droplets in a gas (inset Fig. 1) that can be produced using adapted injectors whatever the liquid composition (liquid mixtures or colloids) as well as thermodynamic properties [7]. In addition, it is possible to inject the precursors with an accurate flow control, a key point for multifunctional nanocomposite thin film processing [8].

Conventionally, aerosols are produced by nebulization or by bubbling [8]. These two methods provide a continuous flow of droplets in the plasma phase, which results in the creation of a so-called misty plasma [29,31], by analogy with dusty plasmas [11]. It means that additional charge losses on liquid droplet surfaces can affect the plasma density and electron temperature, affecting the ionization rate and, consequently, the deposition rate.

Pulsed injection can smooth such effects. Indeed, even if the pulsed injection temporary introduce droplets in the plasma phase, a stationary state can be restored between pulses [12]. This can optimize the plasma deposition process.

Pulsed injection is compatible with low- as well as atmospheric pressure processes as recently reported [12],[14]. But, it introduces new mechanisms related to pulsed gas flow, power injection and plasma-droplets interactions. This paper aims to discuss some of these aspects of pulsed aerosol assisted plasma deposition processes.

## 2. Experimental

As illustrated in Fig. 2, the set-up consisted in two-stage connected to the plasma chamber.

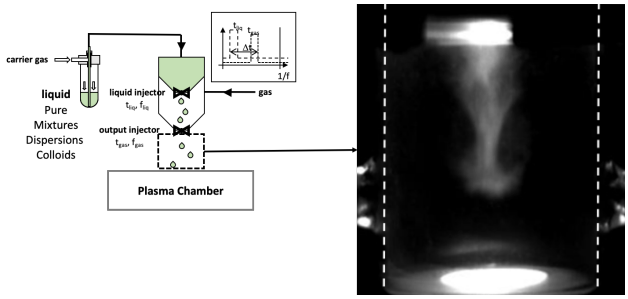


Fig. 2. Schematic of the pulsed injection system.

The aerosol is generated by opening the liquid and the exhaust injectors using appropriate opening times, $t_{liq}$ and $t_{gas}$, and frequencies, $f_{liq}$ and $f_{gas}$ (generally, $f_{gas} = f_{liq} = f$). In the following, we will write the injection conditions as {$t_{liq}$ (in ms) / $t_{gas}$ (in ms) / $f$ (in Hz)}.

Here, the pulsed injection system was coupled to an asymmetric low-pressure RF capacitive discharge [15] and a Dielectric Barrier Discharge at atmospheric pressure [16]. Samples were collected for ex-situ characterization. The thickness was determined by profilometry (Tencor, Alpha Step IQ), and the morphology was probed by Atomic Force Microscopy (AFM BRUKER Multimode 8) in tapping mode and by transmission electron microscopy (MET JEOL JEM 1400 ORIUS).

The pulsed injection induces temporal variations of the process parameters. The effects of pulsed gas flow were simulated by Fluent or Comsol [14] and evidenced on the working pressure measured on a Baratron relative gauge, as well as on electrical characteristics (current, voltage, self-bias) measured on oscilloscopes.

## 3. Nanocomposite thin films

As previously mentioned, pure liquids, mixtures, dispersions or colloidal solutions can be pulsed injected. The latter's enable to form nanocomposite thin films either at low pressure or atmospheric pressure.

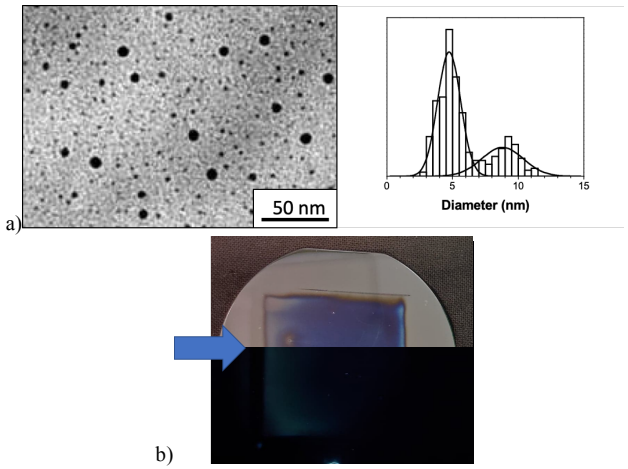


Fig. 3. Coatings obtained with the pulsed injection of a colloidal solution {5/10/1}. a) TEM image of nanocomposite thin film deposited at low-pressure and nanoparticle size distribution. b) picture of nanocomposite thin film obtained at atmospheric pressure (the bottom image was taken under UV irradiation).

First, colloidal solutions are used. It consists in fluorescent ZnO nanoparticles of 6 nm in diameter dispersed in pentane. Fig. 3.a shows a typical TEM image of the nanocomposite thin film obtained at low-pressure. It shows a high dispersion of nanoparticles in the matrix. However, the size distribution reported in Fig. 3.a highlights the presence of two populations of nanoparticle size around 6 and 10 nm. While the first one corresponds to the initial nanoparticles, the second population suggests that nanoparticles aggregates during the process and, especially, in the droplets. Fig. 3.b reports pictures of the nanocomposite thin film deposited in a DBD. The coating limited to the region in-between the electrodes is homogeneous. However, the image taken under UV irradiation (bottom of Fig. 3.b) show a slight fluorescence characteristic of a small quantity of nanoparticles embedded in the matrix.

Recently a secured general synthetic methodology adapted to the formation of nanocomposite thin films has been developed. This approach, called pulsed direct liquid reaction-injection (DLRI) allows the safe-by-design in situ synthesis of nanoparticles prior to their direct injection as an aerosol [19]. DLRI is compatible with various processes including plasmas [20]. The TEM image of the nanocomposite thin film deposited at low-pressure (Fig. 4.a), show a ZnO/DLC nanocomposite with inclusions of well-dispersed, non-aggregated nanoparticles with an average diameter of 6 nm. At atmospheric pressure, Fig. 4.b shows that the coating takes place in the region in-between the electrodes but, the image taken under UV irradiation (bottom of Fig. 4.b) show a higher fluorescence at the entrance of the discharge. It means that nanoparticles are rapidly deposited on the substrate while the matrix deposition takes place all along the discharge cell.

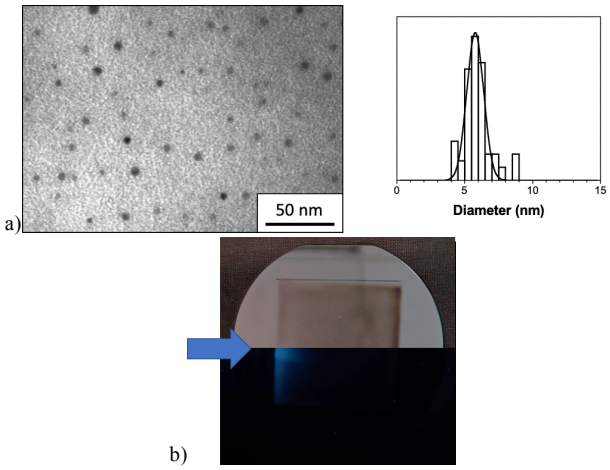


Fig. 4. Coatings obtained with the pulsed direct liquid reactor-injector of nanoparticles (DLRI). a) TEM image of nanocomposite thin film deposited at low-pressure and nanoparticle size distribution. b) picture of nanocomposite thin film obtained at atmospheric pressure (the bottom image was taken under UV irradiation).

These two examples show that pulsed injection enable to form original nanocomposite thin films. However, the pulsed mode induces a lot of mechanisms (flow, transport, discharge) that must be investigated as in the following.

## 4. Pulsed gas injection

Depending on the plasma device, the pulsed injection modifies the gas flow. Fig. 5 reports two numerical simulations obtained for pulsed injections in a) a tube at low-pressure and b) a plane-to-plane discharge cell at atmospheric pressure fed by a gas diffuser.

Pulsed gas injection induces a sharp increase of the gas flow velocity, up to Mach 1 at low-pressure (Fig. 5.a) and by a factor 30 at atmospheric pressure [14]. It thus directly affects the gas transport, at least, its residence time for a

brief moment in the plasma discharge. While this perturbation is transient at low-pressure, pulsed injection can also induce gas recirculation as shown at atmospheric pressure when diffuser is used to inject gas from a pipe to a plane-to-plane discharge (Fig. 5.b). The diffuser act then as a reservoir of gases that can be further introduced in the discharge cell with contaminants from walls [14].

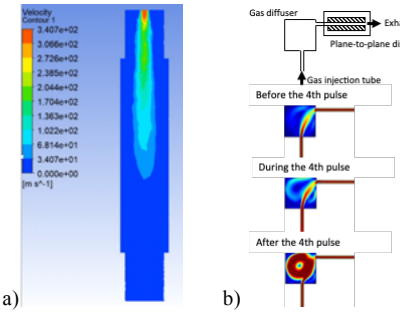


a) b)

Fig. 5. Gas flow simulations of a pulsed gas flow in a) a tube at low-pressure and b) a two plane-to-plane DBD at atmospheric pressure.

Finally, the balance between gas injection and pumping can affect the working pressure, especially in processes at low-pressure. For example, Fig. 6.a reports the time evolution of the pressure with an argon pulse in a RF capacitive discharge fed by a shower head. Two main phases can be observed. In the first 100 ms, the pressure rises according to the pulsed injection of argon (10 ms) and the head losses induced by the showerhead. After 200 ms, the pressure saturates ($p_{max}$ ~ 0.1 mbar) and starts to decrease down to the initial pressure ($p_{min}$ ~ 0.03 mbar). Considering $Q_{Ar}$ the pulsed argon flow rate and $S_p$ the pumping speed on the whole reactor volume $V$, these variations of the pressure can be modelled by [9]:

$$\frac{dp}{dt} = \frac{Q_{Ar}}{V} - \frac{S_p}{V} \cdot p \qquad (1)$$

Integrating equation 1 leads to the dashed curves in Fig 6.a in really good agreement with the experimental data. Hence, for a given system, $p_{max}$ and $p_{min}$ are only function of the gas flow rate, *i.e.* of the pulsed injection parameters.

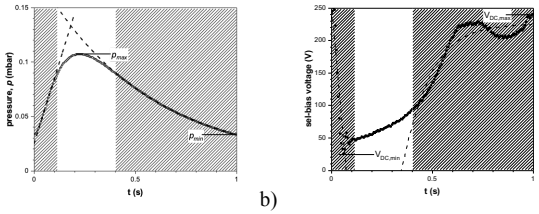


a) b)

Fig. 6. Time evolutions of a) the working pressure and b) the self-bias voltage with a pulsed injection of argon {5/10/1} in an asymmetric RF capacitive discharge –vacuum pressure $10^{-3}$ mbar

As a consequence of the time variations of the pressure, the discharge is pulsed. It is observed for example on the variations of the self-bias voltage. Fig. 6.b shows similar temporal evolutions than of the pressure with a decrease, in absolute value, from a maximal value ($V_{DC,max}$ ~ -225 V) down to ($V_{DC,min}$ ~ -25 V) about 50 ms after the pulse. This phenomenon attributed to the variations of the electron temperature [12] can be modelled by a law scale (dashed curve in Fig. 6.b) related to the particle balance of charged species where electrons and ions are mostly produced by electron-impact ionization of ground state argon atoms and lost by ambipolar diffusion and recombination on plasma reactor walls [12]. Of note, this model does not fully reproduce the experimental curves. Indeed, as the impedance matching box needs to be set in automatic mode to maintain the discharge on, power injection is not constant and oscillate along the pulse period. Injections at higher frequency or with a continuous argon flow allow to fully smooth the effects of pulse injection. In that condition, neither the pressure nor the electrical parameters present time variations [17]. Of note, the resulting working pressure is generally higher (in the Torr range) reducing ion bombardment.

Though the pressure does not vary, pulsed injection also modifies the discharge at atmospheric pressure. Indeed, while continuous injection of nitrogen enables to form homogeneous Townsend discharge, successive pulsed injections turns the discharge into filamentary regime. A key role of contaminant has been reported [14].

## 5. Pulsed aerosol injection

In this part, pentane is injected as an aerosol. It consists in liquid droplets as evidenced by rapid imaging (inset Fig. 1) sprayed with argon for low-pressure RF discharge or with nitrogen for DBD. With {5/10/f}, the volume of pentane injected per pulse is of about 6 µL.

Droplets can be evidenced by light scattering: at atmospheric pressure, they are located in the discharge cell, in between the two electrodes suggesting that they are charged and electrostatically confined as long as the transversal neutral gas force managed by the continuous gas flow is low enough [16]. As the discharge volume is larger, it is less obvious to observe droplets at low-pressure and indirect method must be used.

To investigate the role of liquid droplets, the time variations of the pressure in pentane/argon and argon are compared in Fig. 7.a. With the aerosol and in comparison with argon (grey points), the pressure variation is increased (from $p_{min}$ ~ 0.03 mbar up to $p_{max}$ ~ 0.12 mbar), the saturation is reached sooner (maximum reached 150 ms after the pulse) and equation 1 does not fully reproduce the experimental data (dashed region in Fig 7.a). This phenomenon is even more noticeable with pulsed injection of pentane droplets through single-stage injectors, *i.e.* when $Q_{Ar}$ = 0 (Fig. 5.b). It needs to consider droplet evaporation as reported in [9] *i.e.* the production of pentane vapour from the surface of the liquid droplets. Integrating Equation 1 with liquid droplet evaporation considering a $R^2$ law [18] gets closer the experimental data (solid curve

in Fig. 7.a). It means that liquid pentane lingers for few hundred of ms in the discharge.

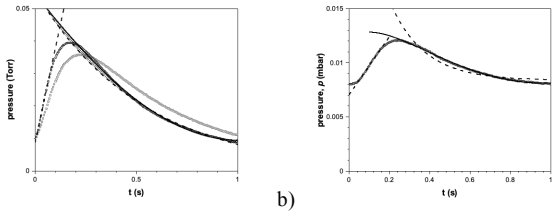


a) b)

Fig. 7. Time evolutions of the pressure with a pulsed injection a) pentane/argon {5/10/1} and b) pentane {5/0/1}.

At a given $t_{liq}$, the volume of liquid injected per pulse is constant but the resulting liquid flow rate, $Q_{liq}$, corresponding for a given size to the number of liquid droplets, increase proportionally to the injection frequency. Considering the previous discussion, it will increase the role of droplet evaporation on the pressures. Fig. 8.a reports the evolution of the extreme values of the pressure: both $p_{min}$ and $p_{max}$ are growing (from 0.1 to 10 Hz, by a factor 30 and 4, respectively) while the difference decreases. Consequently, the extreme values of the self-bias voltage ($V_{DC,min}$ and $V_{DC,max}$) varies with the frequency (Fig. 8.b), *i.e.* with the working pressure as classically reported in low pressure RF plasmas. This behavior may lower the deposition rate and increase the film roughness [1],[2].

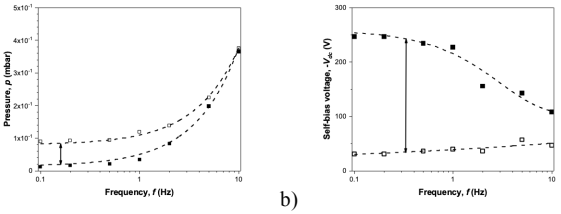


a) b)

Fig. 8. Evolutions of the extreme values of a) the pressure and b) the self-bias voltage with pulsed injections of pentane/argon {5/10/*f*}.

Samples were then collected for the different injection frequencies. However, neither the deposition rate (found around 10 nm.min$^{-1}$) nor the surface roughness (about 0.5 nm) do significantly change with the frequency. Considering the deposition rate, it suggests that the type and the density of reactive species do not change with the neutral density. In addition, ion bombardment may not contribute to the film deposition. Hence, aerosol assisted plasma deposition process does not operate as a classical PE-CVD process. Indeed, the morphology of these thin films are quite different (Fig. 9). At low-pressure, AFM images (Fig. 7.a show the presence of spherical nodules deposited on the film. These spheres are attributed to droplets confined and treated in the plasma volume that deposit on the substrate. In comparison, the viscous structure of the coating formed at atmospheric pressure is attributed to pentane droplets deposition forming a viscous droplet-like film (Fig. 8) [16]. It suggests that plasma-droplets interactions are key mechanisms.

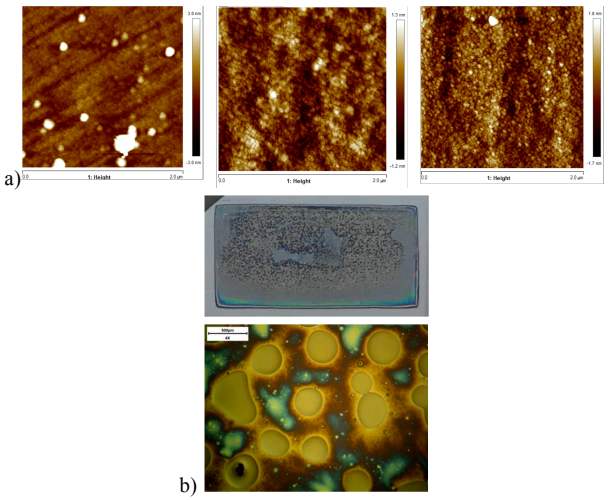

a) b)

Fig. 9. Morphology of the coatings obtained with pulsed injections of pentane/argon a) {5/10/*f*} for $f$ = 0.1, 1 and 10 kHz at low pressure and b) {5/10/0.1} at atmospheric pressure.

## 6. Conclusion

Aerosol-assisted plasma deposition process are appealing method to deposit (multi)functional coatings. However, the physics of such misty plasma is complex and needs an overall study of the different mechanisms.

## 7. References


[1] M. Loboda, *et al.*, *MRS Online Proceed. Lib.*, vol. 447, 1996.
[2] P. Supiot, *et al.*, *Plasma Process. Polym.*, 3, 100, 2006.
[3] A. Bousquet, *et al.*, *Surf. Coat. Technol.*, 200, 6517, 2006.
[4] Y. Gazal, *et al.*, *J. Appl. Phys.*, 121, 123301, 2017.
[5] R. Cozzolino, *et al.*, *Surf. Coat. Technol.*, 205, S198, 2011.
[6] H. Suhr *et al.*, *J. Phys. Coll.*, 50, C5-739, 1989.
[7] F. Palumbo, *et al.*, *Coatings*, 10, 440, 2020.
[8] M. Mitronika, *et al.*, *SN Appl. Sc.*, 3, 1, 2021.
[9] D. Ogawa, *et al.*, *J. Vac. Sci. Technol. A*, 27, 342, 2009.
[10] M. Coppins, *Phys. rev. lett.*, 104, 065003, 2010.
[11] V. Fortov, *et al.*, *Phys. rep.*, 421, 1, 2005.
[12] T. Sadek *et al.*, *Atoms*, 10, 147, 2022.
[14] L. Cacot *et al.*, *J. Phys D: Appl. Phys.*, 55, 445204, 2022
[15] Y. Champouret, *et al.*, *Proceed. 23rd ISPC*, Montréal, Canada, 2017.
[16] L. Cacot, *et al.*, *Plasma Process. Polym.*, DOI 10.1002/ppap.202200165, 2022.
[17] T. Sadek, *et al.*, *Proceed 24rd ISPC*, 2019.
[18] D. Jakubczyk, *et al.*, *Acta Phys. Pol. A*, 122, 709, 2012.
[19] G. Carnide *et al.*, *Adv. Sc.*, p. 2204929, 2022.
[20] G. Carnide *et al.*, submitted to *Coatings*.